Magnetic Resonance Imaging (MRI) as a Method to Investigate Movement of Water During the Extrusion of Pastes

Gil Tomer,[1,3] John Michael Newton,[1] and Paul Kinchesh[2]

Received September 3, 1998; accepted February 9, 1999

Purpose. To assess the potential of Magnetic Resonance Imaging (MRI) as a method of detecting water movement during the extrusion of pastes.

Methods. Plug samples were made from mixtures of model materials and microcrystalline cellulose with two water contents at two different ram speeds to simulate ram extrusion. The extrusion process was stopped at different stages and analyzed for water distribution using MRI to assess the influence of water content and the speed of ram on water movement as the extrusion process progresses.

Results. Two types of water movement were detected: *vertical* and *radial*. When extruding at the faster ram speed, water moved predominantly in the vertical direction, whereas when extruding at a slower ram speed it moved predominantly in the radial direction. At the beginning of the extrusion process a greater water movement in the wetter formulations was observed.

Conclusions. MRI appears to be a useful approach to non-invasive water mapping, and is expected to contribute towards a greater understanding of the role of water in the extrusion of pastes.

KEY WORDS: extrusion; spheronization; water movement; magnetic resonance imaging (MRI); water mapping.

INTRODUCTION

Extrusion

The extrusion process is used in several different industries to manufacture a wide range of products, such as: rubber, plastic, explosives and foods. The pharmaceutical industry uses this process as the first phase of a bi-stage process for the production of pellets, by placing the extrudates on a spheroniser's rotating plate which chops and rounds the extrudates to spherical pellets. The extrusion process involves a major contribution from the liquid component in the system, normally water. The liquid acts as a lubricant, hence at higher water contents, the force required to push the wet mass through the die is lower. In addition, an increased water content decreases the plasticity, reducing the force necessary to extrude the paste (1). It is known that water moves at a higher rate than the solids, usually resulting in extrudates which are wetter than the original wet mass (2,3). Due to the high pressures involved; steel equipment is required which makes it difficult to observe what happens to the liquid during the process.

The existence of convergence patterns in the extrusion of pastes has been observed (2,4,5), a fact that emphasises the importance of looking at what happens within the barrel, which is the topic of this paper.

Nuclear Magnetic Resonance Imaging (MRI)

Nuclear magnetic resonance (NMR) is a spectroscopic technique that is used to study nuclei with a non-zero nuclear spin quantum number, such as ^{1}H. In NMR Imaging (MRI) both a uniform magnetic field, B_0, and a magnetic field gradient, G, are applied across the sample, in form of radio frequency (RF). Application of an RF pulse immediately before switching on gradient G results in an NMR signal with frequency (ω) that depends on the spatial distance(r) in the direction of the applied gradient according to:

$$\omega_{(r)} = \gamma B_0 + \gamma G \cdot r \qquad (1)$$

Where γ is the magnetogyric ratio for ^{1}H, a unique constant to the nucleus being studied, and h is Planck's constant. An experiment of this kind results in 1D projection of the sample along the direction of the applied gradient. In order to generate a series of 2D image slices through a sample it is necessary to use an experiment such as the one represented diagrammatically in Fig. 1. The figure shows when the RF pulse is applied and when the NMR signal is acquired in relation to the application of gradients in the directions of G_{read}, G_{phase} and G_{slice} which are mutually perpendicular to each other.

When a gaussian shaped RF pulse is applied in the presence of gradient G_{slice}, it selectively excites a slice within the sample that is perpendicular to the direction of the gradient. By stepping the frequency of the RF pulse, a series of contiguous slices can be sampled. Spatial information in the directions of G_{read} and G_{phase} is encoded within the NMR signal by application of gradients G_{read} and G_{phase} respectively. The spatial information is unravelled by performing a 2D Fourier Transformation (2DFT) of the data acquired from each slice thus giving a series of 2D images.

The intensity of the NMR signal at time *te* (echo time), which, in general, is a function of the relaxation times T_1 (spin-lattice relaxation time constant) and T_2 (spin-spin relaxation time constant) as well as the proton concentration, is the actual measurement being made in these experiments. The intensity of the observed magnetisation generated immediately after the 90° excitation pulse (I_0) is proportional to the proton concentration when the repetition time, *tr*, is sufficiently long to allow full relaxation of the NMR signal. When *tr* does not allow complete relaxation, then the NMR signal becomes saturated and the intensity of the observed magnetisation generated immediately after the 90° excitation pulse has intensity I_s, where $I_s < I_0$. The equilibrium value of I_s immediately following a

[1] Pharmaceutics Department, School of Pharmacy, University of London, 29-39 Brunswick square, London WC1N 1AX, UK.

[2] ULIRS NMR Imaging and Spectroscopy, Department of Chemistry, Queen Mary and Westfield College, University of London, London E1 4NS, UK.

[3] To whom correspondence, should be addressed. (e-mail: gtomer@ulsop.ac.uk)

0724-8741/99/0500-0666$16.00/0

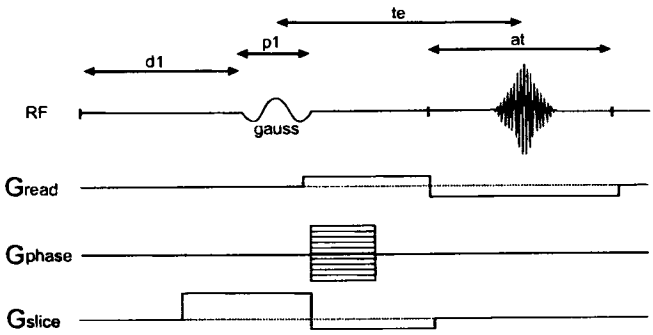

Fig. 1. A diagrammatic representation of the different gradient and RF signals involved in the MRI experiments (d1 = relaxation time [s], p1 = pulse duration [μs], te = echo time [ms], at = acquisition time [ms]). The horizontal scale represents the timing of the experiment. The three gradients are perpendicular to each other.

pulse in a train of identical 90° pulses separated by time τ is given by (6):

$$I_s = I_0 \frac{1 - \exp\left(\frac{-\tau}{T_1}\right)}{1 + \exp\left(\frac{-\tau}{T_1}\right)\exp\left(\frac{-\tau}{T_2}\right)} \quad (2)$$

In a train of identical 90° pulses all that happens during time τ is that the magnetisation relaxes in the presence of the main magnetic field B_0 only. In the MRI experiment used in this study, τ corresponds to the $(tr - te)$, since at the time te after the initial 90° excitation pulse, the net magnetisation points in exactly the same direction as immediately after the initial 90° excitation pulse, the only difference being in magnitude, which, as a result of T_2 relaxation, has decayed according to:

$$I_{te} = I_0 \exp\left(\frac{-te}{T_2}\right) \quad (3)$$

The observed intensity after time te is, therefore, given by:

$$I_{te} = I_s \exp\left(\frac{-te}{T_2}\right) \quad (4)$$

To all intense and purposes, the observed intensity in the MRI experiment is, therefore, given by re-evaluating equation (2) in the $\tau \gg T_2$ limit and substituting the result into equation (4) with τ, i.e.

$$I_{te} \approx I_0 \left[1 - \exp\left(\frac{-\tau}{T_1}\right)\right]\left[\exp\left(\frac{-te}{T_2}\right)\right] \quad (5)$$

The advantages of using MRI are:

1. It is non-destructive and non-invasive method.
2. It can be selective to a certain region of the sample.
3. It can give the relative concentration as a function of spatial location.

MRI is extensively used for medical imaging. It has been used also for mapping of liquids in solid objects in many different fields of research, e.g. residual water in dolomite cores (7), swelling of hydrating HPMC tablets (8,9), the effect of drug on buffer uptake kinetics in polymers (10), mapping of water during extrusion of ceramic pastes (11), flow mapping of solid rock fuel (12), blood thorough blood vessels (13) and flow patterns in screw extruders (14).

Flow visualisation using MRI is more appropriate for steady state flows (15), which is not the case with extrusion where convergence is a common phenomena near the die (2,5).

MATERIALS AND METHODS

Two different esters of gallic acid, methyl-paraben (Nipa Laboratories, Mid Glamorgan, UK) and propyl-paraben (Nipa Laboratories, Mid Glamorgan, UK) were mixed with microcrystalline cellulose (Avicel PH-101, FMC, Cork, Ireland) in the proportion of 7 parts to 5 parts to which water was added (formulation K: 40% of the total mass and formulation Q: 45.45% of the total mass). The wet mass was extruded using a ram extruder (16) (2.54 cm diameter barrel) fitted with a single-hole die, 1mm diameter and 4mm in length, at a speed of 200 mm/min and 20 mm/min, driven by a mechanical press (Lloyds MX-50, Southhampton, UK). From each formulation four different plugs were examined, produced by stopping the extrusion process after 5.5, 13.5, 21.5 and 29.5 mm of piston displacement. The plugs were wrapped in a plastic bag to prevent evaporation of water. The plugs were examined, within one hour after extrusion, using MRI experiments which were performed using a SISCO-200 (Varian-Siemens, Palo Alto, California, USA) NMR imaging spectrometer equipped with an Oxford 200/330 MkII 33 cm horizontal bore superconducting magnet with maximum gradient strength of 10 G/cm (Oxford Instruments, Oxford, UK) and Oxford 15 channel shims (Oxford Instruments, Oxford, UK). Data was acquired with Varian's VnmrX_5.1a software on a Super Workstation 5 (SPARC5 clone) and analyzed with XDISPUNC image processing software (UCLH UCL Hospitals NHS Trust, London, UK). The parameters used for data acquisition, as shown in figure 1, were set to the following values: delay(d1) = 0.041 s, repetition time(tr) = 2.4 s, echo time(te) = 2.5 ms, pulse duration(pl) = 1000 μs and acquisition time(at) = 2.6 ms. The echo time of 2.5 ms was achieved by reducing the strength of the initial dephasing gradient lobe in direction G_{read}. This had the desired effect of forcing the NMR signal to refocus earlier in the acquisition window (17). It is not possible to shorten the echo time employed as the experiment is at the limits imposed by hardware constraints. Furthermore, at

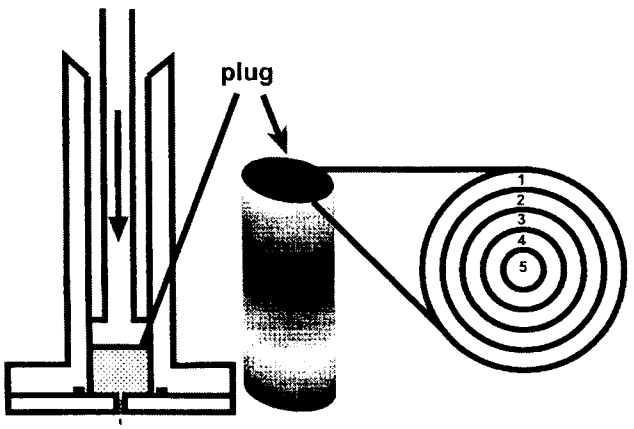

Fig. 2. A diagram describing the subdivision to slices and rings of the plug.

Table 1. T_1, T_2, and Root Mean Square of Signal to Noise Ratios Recorded for the Different Plugs[a]

Material	T_1(sec)	T_2(ms)	I_{te}/I_0	rms signal/noise	% I_{te}/I_0	% rms signal/noise
Methyl Paraben	1.585 ± 0.007	6.4 ± 0.2	0.509 ± 0.001	16.95	0.5%	6%
Propyl Paraben	1.754 ± 0.005	6.0 ± 0.1	0.473 ± 0.001	23.68	0.4%	4%

[a] I_{te}/I_0 is calculated using equation (5) with τ = 2.216 sec and te = 2.5 ms. From those values the variation in signal to noise ratio and I_{te}/I_0 are calculated.

longer echo times, the resulting magnetisation becomes indistinguishable from the noise. As such, it is not possible to obtain quantitative 2D results generated from an exponential fit of each pixel to 2D data acquired at several echo times, as previously described (10). In order to demonstrate that 2D data obtained at a single echo time can be quantified, relaxation measurements were performed spectroscopically to determine bulk sample relaxation characteristics. T_2 measurements were performed using a standard Carr-Purcell-Meiboom-Gill(cpmg) sequence, and T_1 measurements with a standard inversion recovery sequence. 2D image data sets were subsequently acquired with an in-plane spatial resolution of approximately 0.6mm × 0.6mm, a slice thickness of approximately 1mm with no gap between the slices, and 128 accumulations.

The image processing software was used to define five concentric rings of equal thickness in each of the horizontal slices, as dipicted in Fig. 2 and to calculate the accumulative signal intensity from the water in each of the five rings. A relative numerical value is calculated for each ring, which is a representative value for the relative amount of water to those from other slices within the same sample.

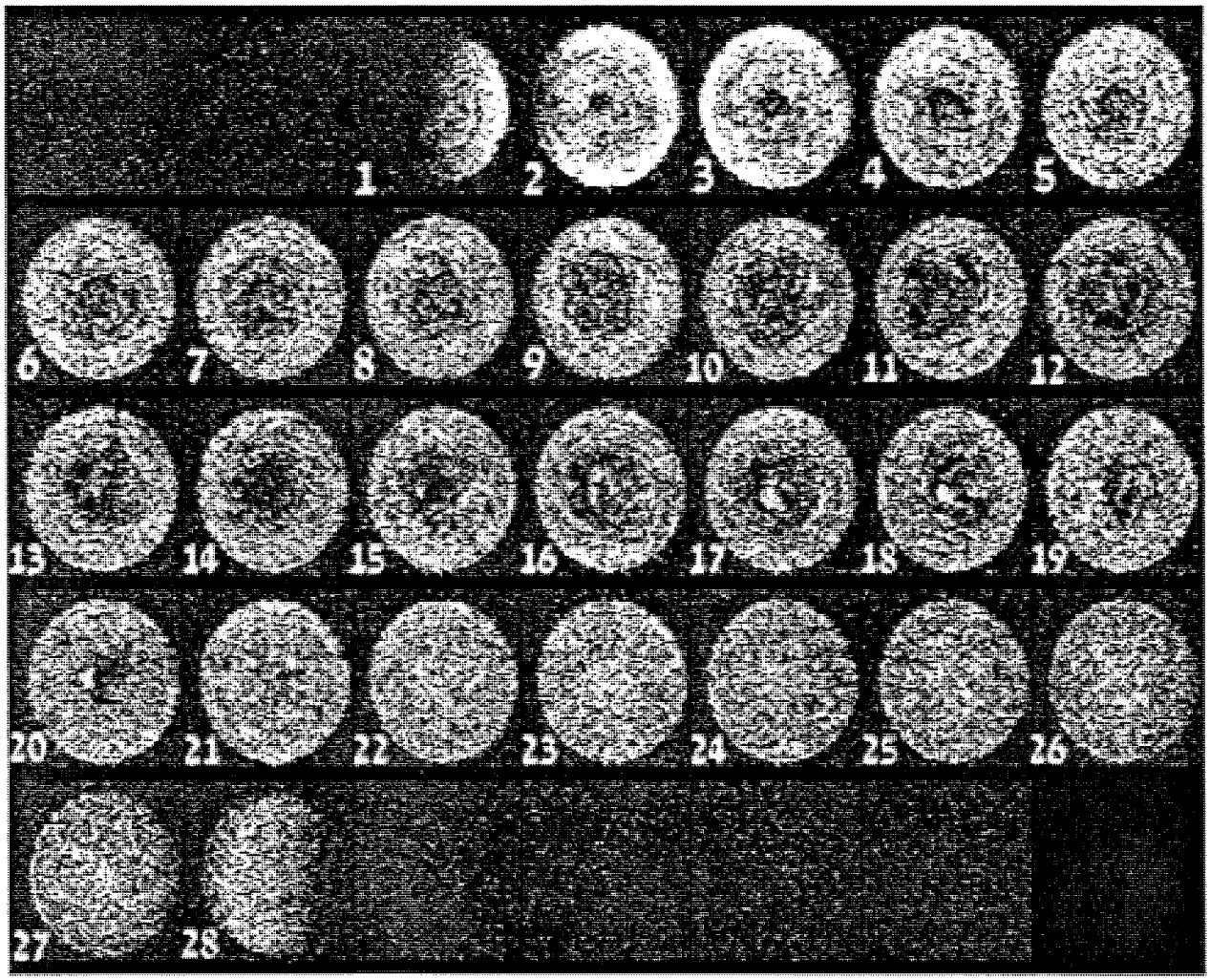

Fig. 3. 2D slices from Methyl-Paraben/MCC 13.5 mm displacement plugs. White dots represent the presence of water. Slice 1 is at the bottom of the barrel (near the die).

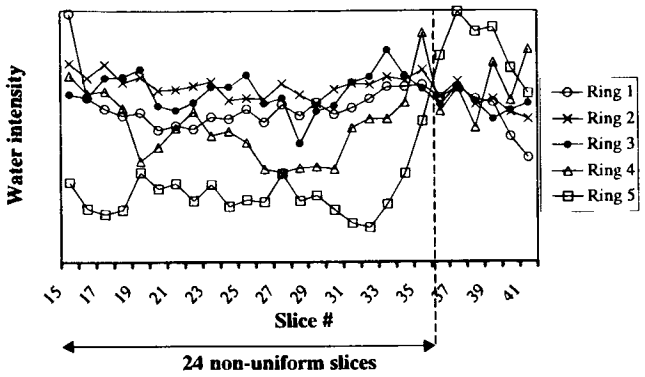

Fig. 4. A sample graph for Propyl Paraben, formulation K that was extruded at 200 mm/min and stopped after 21.5mm of piston displacement. The line marks the point from which the slices are beginning to become uniform.

RESULTS AND DISCUSSION

As each MRI experiment took nearly 12 hours to perform, a series of preliminary experiments were performed to check the reproducibility of the MRI experiment and to ascertain whether there is additional water movement in the sample during the 11 hours and 15 minutes experiment. A plug from each material underwent eight 30 minutes MRI experiments one after the other, followed by three experiments of four hours. The results from the different experiments were compared. The results showed a low coefficient of variation (3.2% on average). One can assume that no or negligible water movement is occurring in the one hour gap between extrusion and MRI examination. In comparison to the extensive water movement which could be induced by the extrusion process, here water movement would be limited to that occurring by diffusion. Therefore, it can be assumed that no water movement occurs during the MRI measurement.

The T_1, T_2 and the root mean square signal to noise ratio values recorded for the plugs of the two materials are displayed in Table 1. From the relaxation time experiments it was found that the data fitted very well to a single exponential decay with both relaxation times experiments. Signal to noise ratio values corresponded to typical images used in this study. It therefore seems sensible to assume that the relaxation properties are approximately uniform throughout the sample. Furthermore, the percentage variation in I_{te}/I_0 is significantly lower than the noise levels in the data to the extent that variations in image intensity resulting from spatial variations in relaxation times are negligible with respect to the noise levels in the data. As such, it is concluded that the data are quantitative within the limits of experimental error. The observed trends in intensity measurements are, therefore, expected to reflect the water concentration distribution within the samples.

The formulations tested have been shown previously by preliminary experiments to be capable of the production of spherical pellets by the process of extrusion/spheronization and therefore represents a 'good' formulation.

A typical set of images is shown in Fig. 3 that represents slices from the bottom to the top of a plug sample. When looking at the moisture content along the length of the plug, clear differences in the distribution of water between the concentric ring subdivisions are observed. Water movement can

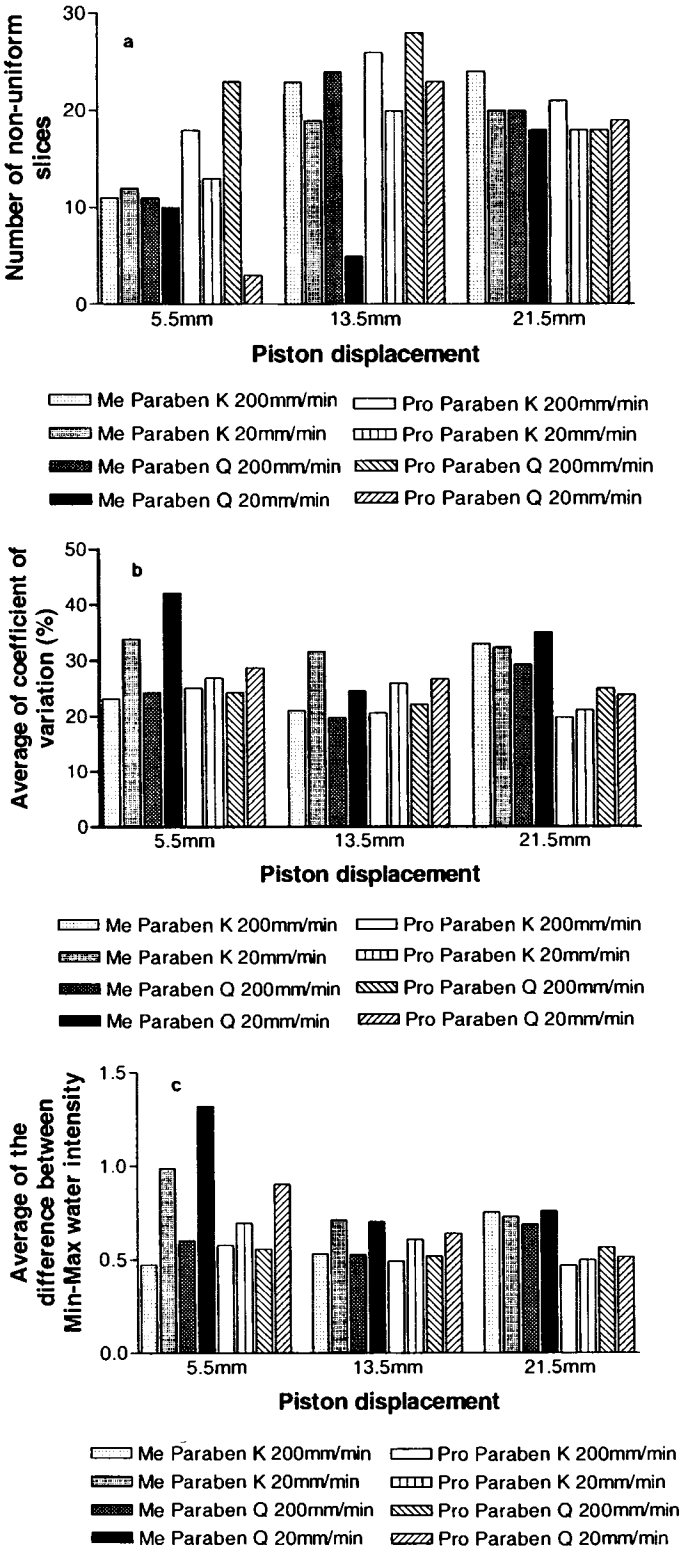

Fig. 5(a). Number of non-uniform slices at the two extrusion speeds (Me = Methyl Paraben, Pro = Propyl Paraben). (b) Average of the coefficient of variation of the water intensity at the non-uniform slices (Me = Methyl Paraben, Pro = Propyl Paraben). (c) Average of the difference between minimum and maximum water intensity at each of the non-uniform slices (Me = Methyl Paraben, Pro = Propyl Paraben).

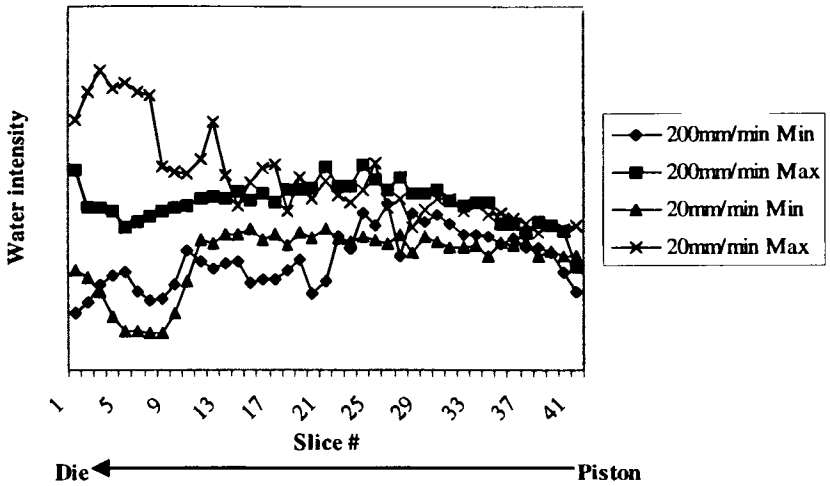

Fig. 6. The difference in water movement between the two extrusion speeds demonstrated by looking only at the value of the minimum and the maximum water intense ring at each slice. The above results are from examining Methyl Paraben/MCC plugs with 40% of water when stopped after displacement of 13.5 mm.

be quantified from these figures in three ways: a) number of non-uniform slices, b) coefficient of variation of the water intensity for the different rings at each slice and c) average of the difference in water intensity of the wettest ring and the driest ring at each slice.

The number of non-uniform slices can be determined by examination of the graph of the water intensity of the different rings of the different slices (Figure 4). From the first slices, the lines representing the water intensity at the different rings are scattered, until they reach a point from which all the lines converge. This point, marked on Fig. 4 with a dotted line, is the point from which all the slices are relatively uniform in water content. Examining the coefficient of variation of each slice can also identify this point. A steep decline in the coefficient of variation value is recorded, in most cases from levels of 20%–40% to below 10% (see Fig. 5b).

As the extrusion process was allowed to continue further, it was noted that the number of slices which had large differences of water content between the different rings (i.e. non-uniform slices) was larger.

Furthermore, through all the non-uniform slices, the most inner ring is the driest of the rings. The above phenomenon is related to water movement in two directions: a) *vertical movement*—when water is moving down the barrel towards the die and b) *radial movement*—when water is moving from the center of the barrel towards the walls of the barrel, which leaves the inner ring relatively dry. When looking at the bottom slices (i.e. near the die) a dramatic increase in water content at the outer rings is recorded. This is probably occurs due to water being trapped at the sides of the die and accumulating there. This can occur due to convergence at the sides of the die, a phenomenon which was first reported in extrusion of low-density polymers by Tordella (18) and later was observed to occur also in extrusion of pharmaceutical pastes (2,5).

When the extrusion process was stopped at a later stage for the slower speed, the plug examined is much drier, hence the plugs produced after 29.5 mm of piston displacement were too dry for the water to be imaged, given current instrumental constrains. The results from the 29.5mm displacement were, therefore, not included in this paper.

When comparing the results for the two different extrusion speeds, a difference in the extent of the water movement can be seen in both formulations. In the case of the faster speed (200 mm/min), the water moves more rapidly vertically (when looking at the number of non-uniform slices—Figure 5a). In the case of the slower speed (20 mm/min), the water moves faster in the radial direction, as indicated from either the coefficient of variation between the rings in the non-uniform slices represented in Figure 5b, or the average of the difference between the maximum and minimum water intensity in each slice represented in Figure 5c. Figure 6 demonstrates the difference in water content between the wettest and the driest rings in each horizontal slice of one of the plugs. The difference of direction of water movement between the two extrusion speeds can be related to the fact that extrusion at slow speed allows the water more time to spread in the radial direction and fill all the space between the particles, whereas at the faster speed the water does not have time to move and therefore the space is filled by water coming down from the top layers of the barrel.

When comparing the water movement between the two formulations, one can see that at the beginning of the extrusion (after displacement of 5.5mm) there is more water movement both in the radial and in the vertical direction in the wetter formulation (Q)—Figs. 5a–5c. Nevertheless, as the process progresses (displacements of 13.5 mm and 21.5 mm) no obvious difference is seen in the extent of the water movement between the two formulations.

CONCLUSIONS

The results of the MRI experiments presented here support the previous observations of this process, especially the liquid movement within the barrel. Furthermore, this method is sensitive enough to distinguish between two different types of water movements (vertical and radial), which has not been possible with other methods.

movement within the barrel. Furthermore, this method is sensitive enough to distinguish between two different types of water movements (vertical and radial), which has not been possible with other methods.

In conclusion, the MRI technique appears to be a suitable tool for tracking water movement inside the barrel during the extrusion process, hence suitable for evaluating the extent of water mobility within potential formulations.

ACKNOWLEDGMENTS

The imaging spectrometer was provided by the University of London Intercollegiate Research Service scheme and is located at Queen Mary and Westfield College. G.T. would also like to thank the Overseas Research Students (ORS) scholarship scheme and the Leo Baeck scholarship for their support.

REFERENCES

1 P. J. Harrison, J. M. Newton, and R. C. Rowe. The characterization of wet powder masses suitable for extrusion/spheronization. *J. Pharm. Pharmacol.* **37**:686–691 (1985).
2 K. E. Fielden, J. M. Newton, and R. C. Rowe. The effect of lactose particle size on the extrusion properties of microcrystalline cellulose-lactose mixtures. *J. Pharm. Pharmacol.* **41**:217–221 (1989).
3 L. Baert, J. P. Remon, P. Knight, and J. M. Newton. A comparison between the extrusion forces and spheres quality of a gravity feed extruder and a ram extruder. *Int. J. Pharm.* **86**:187–192 (1992).
4 P. J. Harrison. Extrusion of wet powder masses. *PhD Thesis, University of London.* (1982)
5 P. J. Harrison, J. M. Newton, and R. C. Rowe. Convergent flow analysis in the extrusion of wet powder masses. *J. Pharm. Pharmacol.* **36**:796–798 (1984).
6 P. T. Callaghan. *Principles of nuclear magnetic resonance microscopy.* Clarendon Press, Oxford, 1993: p. 79.
7 G. C. Borgia, A. Brancolini, A. Camanzi, and G. Maddinelli. Capillary water determination in core plugs: a combined study based on imaging techniques and relaxation analysis. *Magn. Res. Imag.* **12**:221–224 (1994).
8 A. R. Rajabi-Sihboomi, R. W. Bowtell, A. Henderson, M. C. Davies, and C. D. Melia. Structure and behaviour in hydrophilic matrix systained release dosage forms: 2. NMR-imaging studies of dimensional changes in the gel layer and core of HPMC tablets undergoing hydration. *J. Cont. Rel.* **31**:121–128 (1994).
9 M. Kojima, S. Ando, K. Kataoka, T. Hirota, K. Aoyagi, and H. Nakagami. Magnetic resonance imaging (MRI) study of swelling and water mobility in micronized low-substituted hydroxypropylcellulose matrix tablets. *Chem. Pharm. Bull.* **46**:324–328 (1998).
10 T. M. Hyde, L. F. Gladden, and R. Payne. A nuclear magnetic resonance imaging study of the effect of incorporating a macromolecular drug in poly(glycolic acid-DL-lactic acid). *J. Contr. Rel.* **36**:261–275 (1995).
11 J. Gotz and H. Buggisch. NMR imaging of pastes in a ram extruder. *J. Non-Newtonian Fluid Mech.* **49**:251–275 (1993).
12 S. W. Sinton and A. W. Chow. NMR imaging for studies of suspension rheology. *Paper presented at Society of Rheology, Sante Fe, NM.* 21–25 October (1990).
13 G. T. Gullberg, M. A. Simons, F. W. Wehrli, and D. N. G. Row. Time-of-flight NMR imaging of plug and laminar flow. *SPIE physics and engineering of computerized multidimensional imaging and processing.* **671**:314–319 (1990).
14 C. K. Agemura, R. J. Kautenand, and K. L. McCarthy. Flow fields in straight and tapered screw extruders using magnetic resonance imaging. *J. Food Eng.* **25**:55–72 (1995).
15 L. F. Gladden. Nuclear magnetic resonance in chemical engineering: principles and applications. *Chem. Eng. Sci.* **49**:3339–3408 (1994).
16 A. Ovensten, J. J. Benbow. Effects of die geometry on extrusion. *Trans. Br. Cer. Soc.* **67**:543–567 (1968).
17 P. Kinchesh, D. S. Powlson, E. W. Randall, and S. C. R. Williams. NMR imaging of ^{14}N in solution. *J. Magn. Reson.* **97**:208–212 (1992).
18 J. P. Tordella. Unstable flow of molten polymers. In R. E. Frederick (ed.), *RHEOLOGY: Theory and Application*, Academic press: New-York and London, 1969, pp. 57–92.